Nanoscale

PAPER

View Article Online
View Journal | View Issue

Cite this: *Nanoscale*, 2017, **9**, 6521

Cooperative and non-cooperative sensitization upconversion in lanthanide-doped $LiYbF_4$ nanoparticles†

Qilin Zou,[a,b] Ping Huang,[a] Wei Zheng,* [a,b] Wenwu You,[a] Renfu Li,[a] Datao Tu,[a,b] Jin Xu[a] and Xueyuan Chen*[a,b]

Received 25th March 2017,
Accepted 6th April 2017

DOI: 10.1039/c7nr02124k

rsc.li/nanoscale

Lanthanide (Ln^{3+})-doped upconversion nanoparticles (UCNPs) have attracted tremendous interest owing to their potential bioapplications. However, the intrinsic photophysics responsible for upconversion (UC) especially the cooperative sensitization UC (CSU) in colloidal Ln^{3+}-doped UCNPs has remained untouched so far. Herein, we report a unique strategy for the synthesis of high-quality $LiYbF_4$:Ln^{3+} core-only and core/shell UCNPs with tunable particle sizes and shell thicknesses. Energy transfer UC from Er^{3+}, Ho^{3+} and Tm^{3+} and CSU from Tb^{3+} were comprehensively surveyed under 980 nm excitation. Through surface passivation, we achieved efficient non-cooperative sensitization UC with absolute UC quantum yields (QYs) of 3.36%, 0.69% and 0.81% for Er^{3+}, Ho^{3+} and Tm^{3+}, respectively. Particularly, we for the first time quantitatively determined the CSU efficiency for Tb^{3+} with an absolute QY of 0.0085% under excitation at a power density of 70 W cm^{-2}. By means of temperature-dependent steady-state and transient UC spectroscopy, we unraveled the dominant mechanisms of phonon-assisted cooperative energy transfer (T > 100 K) and sequential dimer ground-state absorption/excited-state absorption (T < 100 K) for the CSU process in $LiYbF_4$:Tb^{3+} UCNPs.

1. Introduction

Lanthanide-doped upconversion nanoparticles (UCNPs) that are able to convert two or more low-energy pump photons into one high-energy output photon have recently attracted tremendous interest in the fields of biomedicine and nanomedicine because of their superior physicochemical features and unique optical properties.[1–9] Yb^{3+}, owing to its large absorption cross-section at ~980 nm, is usually selected as a sensitizer in lanthanide (Ln^{3+})-doped UCNPs, which can effectively absorb near-infrared (NIR) photons and transfer the excitation energy to nearby activators to yield efficient upconversion (UC) luminescence.[10–13] For Ln^{3+} activators with stepwise long-lived intermediate energy levels matching those of Yb^{3+}, such as Er^{3+}, Ho^{3+} and Tm^{3+}, resonant or phonon-assisted energy transfer (ET) UC (ETU) occurs easily.[14–17] While for those Ln^{3+} ions without metastable levels as the energy storage reservoir, such as Tb^{3+} and Eu^{3+}, cooperative sensitization UC (CSU) takes place.[18–22] In a typical CSU process, the excitation energy of two adjacent Yb^{3+} is simultaneously transferred to Tb^{3+} or Eu^{3+}.[19] CSU luminescence from activators such as Tb^{3+} or Eu^{3+} is less influenced by the deleterious surface quenching effect than ETU luminescence from Er^{3+} or Tm^{3+}, due to the large energy gap between the emitting levels and their next low-lying levels of Tb^{3+} or Eu^{3+}, thereby demonstrating unique advantages and promises for applications in UC-FRET biodetection and bioimaging.[23–27] Thanks to the pioneering work reported by H. U. Güdel and others in theoretical and experimental studies on CSU,[28–31] much of the spectroscopy and mechanism for the CSU process in bulk materials are well understood. However, in the case of colloidal Ln^{3+}-doped UCNPs, their mechanism has remained unexplored so far.

$LiYbF_4$, due to its low phonon energy (~460 cm^{-1}) and high chemical stability, has been regarded as an efficient host material for UC luminescence (UCL).[32,33] Meanwhile, the sensitizer Yb^{3+} ions as a constituent of the host can not only maximize the absorption but also facilitate energy migration among Yb^{3+} sub-lattices, which may promote ET processes between Yb^{3+} and the activators, thus resulting in distinct UCL characteristics and improved UCL efficiency compared to their

[a]*CAS Key Laboratory of Design and Assembly of Functional Nanostructures, and State Key Laboratory of Structural Chemistry, Fujian Institute of Research on the Structure of Matter, Chinese Academy of Sciences, Fuzhou, Fujian 350002, China. E-mail: xchen@fjirsm.ac.cn, zhengwei@fjirsm.ac.cn; Fax: +86 591 63179421; Tel: +86 591 63179421*

[b]*College of Materials Science and Engineering, Fujian Normal University, Fuzhou, Fujian 350007, China*

†Electronic supplementary information (ESI) available: Tables S1–S3 and Fig. S1–S23. See DOI: 10.1039/c7nr02124k

low-concentration Yb^{3+}-doped counterparts.[34–36] However, due to the stringent synthetic conditions and the surface quenching effect, currently it remains difficult for the synthesis of high-quality $LiYbF_4:Ln^{3+}$ UCNPs with controlled particle size and efficient UCL.

Herein, we report a unique strategy for the synthesis of monodisperse $LiYbF_4:Ln^{3+}$ core-only and core/shell UCNPs with controlled particle sizes and shell thicknesses through a modified high-temperature co-precipitation method. Trioctylamine (TOA) instead of 1-octadecene (ODE), that is commonly used in the synthesis of other Ln^{3+}-doped UCNPs, is utilized as a solvent to provide an elevated reaction temperature for the crystallization and ripening of the UCNPs,[37,38] in view of its higher boiling temperature (365.8 °C) than ODE (314.2 °C) (Table S1†). The resulting core/shell UCNPs yield remarkably enhanced UCL. ETU from Er^{3+}, Ho^{3+} and Tm^{3+} and CSU from Tb^{3+} are systematically surveyed by room-temperature (RT) spectroscopic characterization. Furthermore, by means of low-temperature (10 K) high-resolution steady-state and transient UC spectroscopy, we unravel the excited-state dynamics involved in the CSU process in $LiYbF_4:Tb^{3+}$ UCNPs.

2. Experimental

2.1. Chemicals and materials

$CH_3COOLi{\cdot}2H_2O$, NH_4F, cyclohexane, methanol, and ethanol were purchased from Sinopharm Chemical Reagent Co., China. Oleic acid (OA) and TOA were purchased from Alfa Aesar (China). $Yb(CH_3COO)_3{\cdot}4H_2O$ (99.999%), $Er(CH_3COO)_3{\cdot}4H_2O$ (99.99%), $Tm(CH_3COO)_3{\cdot}4H_2O$ (99.99%), $Ho(CH_3COO)_3{\cdot}4H_2O$ (99.99%), $Tb(CH_3COO)_3{\cdot}4H_2O$ (99.99%) and $Y(CH_3COO)_3{\cdot}4H_2O$ (99.99%) were purchased from Sigma-Aldrich (China). All chemicals were used as received without further purification.

2.2. Synthesis of $LiYbF_4:Ln^{3+}$ core-only UCNPs

The $LiYbF_4:Ln^{3+}$ (Ln = Er, Tm, Ho, or Tb) core-only UCNPs were synthesized *via* a high-temperature co-precipitation method. In a typical synthesis of $LiYbF_4$:30%Tb UCNPs, 1 mmol of $CH_3COOLi{\cdot}2H_2O$, 0.7 mmol of $Yb(CH_3COO)_3{\cdot}4H_2O$ and 0.3 mmol of $Tb(CH_3COO)_3{\cdot}4H_2O$ were mixed with 8 mL of OA and 12 mL of TOA in a 100 mL three-necked round-bottom flask. The resulting mixture was heated to 160 °C under a N_2 flow with constant stirring for 30 min to form a clear solution, and then cooled down to RT. Thereafter, 10 mL of methanol solution containing 4 mmol of NH_4F was added and the solution was stirred at 60 °C for 30 min to remove methanol. After methanol was evaporated, the resulting solution was heated to 320 °C under a N_2 flow with vigorous stirring for 60 min, and then cooled down to RT. The obtained UCNPs were precipitated by addition of 30 mL of ethanol, collected by centrifugation, washed with ethanol several times, and finally re-dispersed in cyclohexane. To control the size and morphology of the UCNPs, the mixed solution was allowed to react at different temperatures (*e.g.*, 300 °C and 310 °C) and for different times (*e.g.*, from 20 min to 120 min).

2.3. Synthesis of $LiYbF_4:Ln^{3+}$@$LiYF_4$ core/shell UCNPs

Briefly, 0.5 mmol of $CH_3COOLi{\cdot}2H_2O$ and 0.5 mmol of $Y(CH_3COO)_3{\cdot}4H_2O$ were added to a 100 mL three-necked round-bottom flask containing 8 mL of OA and 12 mL of TOA. The mixed solution was then heated to 160 °C under a N_2 flow with constant stirring for 30 min to form a clear solution. After cooling down to 80 °C, 0.5 mmol of $LiYbF_4:Ln^{3+}$ core-only UCNPs in 10 mL of cyclohexane was added and maintained at 80 °C for 30 min to remove cyclohexane. After the removal of cyclohexane, 10 mL of methanol solution containing 2 mmol of NH_4F was added and stirred at 60 °C for another 30 min to remove methanol. After methanol was evaporated, the solution was heated to 320 °C under a N_2 flow with vigorous stirring for 60 min, and then cooled down to RT. The resulting core/shell UCNPs were precipitated by addition of 30 mL of ethanol, collected by centrifugation, washed with ethanol several times, and finally re-dispersed in cyclohexane. To control the shell thickness, different amounts of the shell precursors were weighed for the synthesis.

2.4. Characterization

Powder X-ray diffraction (XRD) patterns of the samples were collected with an X-ray diffractometer (MiniFlex2, Rigaku) with Cu Kα1 radiation (λ = 0.154187 nm). Both the low- and high-resolution transmission electron microscopy (TEM) measurements were performed by using a TECNAI G^2 F20 TEM equipped with the energy dispersive X-ray spectrum (EDS). Downshifting luminescence (DSL) emission and excitation spectra and the corresponding photoluminescence (PL) lifetimes were recorded on a spectrometer (FLS980, Edinburgh) equipped with both continuous xenon (450 W) and pulsed flash lamps. UCL emission spectra were acquired under 980 nm excitation with a continuous-wave semiconductor NIR laser diode (2 W). UCL lifetimes were measured with a customized UV to mid-infrared steady-state and phosphorescence lifetime spectrometer (FSP920-C, Edinburgh) equipped with a digital oscilloscope (TDS3052B, Tektronix) and a tunable mid-band Optical Parametric Oscillator (OPO) pulse laser as the excitation source (410–2400 nm, 10 Hz, pulse width ≤5 ns, Vibrant 355II, OPOTEK). The absolute UC quantum yield (QY) was measured on a customized UCQY measurement system combined with a fiber optic spectrometer (QE65pro, Ocean Optics), a standard integrating sphere (150 mm in diameter, Edinburgh), a 980 nm diode laser (MDL-III-980-2W, Changchun New Industries Optoelectronics Tech Co., Ltd) as the excitation source, and a neutral density filter to attenuate the excitation light (for details, please see also the Experimental section and Fig. S1 in the ESI†). A tungsten lamp (100 W, Edinburgh) was used as a correction for the spectral response of the system, and the UCL emission peaks in the spectral region of 460–620 nm for Tb^{3+}, 410–690 nm for Er^{3+}, 330–840 nm for Tm^{3+} and 470–630 nm for Ho^{3+} were integrated for the QY determination. For low-temperature

measurements, samples were mounted on a closed cycle cryostat (10–300 K, DE202, Advanced Research Systems). To avoid laser burning of the samples in a vacuum environment in the closed cycle cryostat, the as-synthesized UCNPs were washed with acid to yield ligand-free UCNPs. PL photographs of the UCNP solutions were taken by using a Canon 70D digital camera without using any filter. All the measurements were carried out by using powder samples, and all the spectral data were corrected for the spectral response of both the spectrometer and the integrating sphere.

3. Results and discussion

3.1. Structure and morphology

The $LiYbF_4$ crystal has a tetragonal structure (space group $I4_1/a$) with the Yb^{3+} ions surrounded by eight F^- ions that form the edges of a slightly distorted dodecahedron (Fig. 1a).[39] All Yb^{3+} ions occupy a single site with a symmetry of S_4. High-quality $LiYbF_4$:Ln^{3+} (Ln = Er, Tm, Ho, or Tb) core-only and core/shell UCNPs were synthesized *via* a modified high-temperature co-precipitation method in the presence of OA and TOA as the surfactant and the solvent, respectively. The as-synthesized UCNPs are hydrophobic and can readily disperse in a variety of nonpolar organic solvents because of the oleic ligands anchored to the surface of the UCNPs. The XRD patterns (Fig. 1b and S2†) show a set of intense and indexed diffraction peaks of tetragonal $LiYbF_4$ (JCPDS No. 71-1211) for both $LiYbF_4$:Ln^{3+} core-only and core/shell UCNPs, indicating the pure phase and the high crystallinity of the UCNPs. Slightly narrower diffraction peaks for core/shell UCNPs than for core-only UCNPs were observed, due to the increase in the particle size of core/shell UCNPs. The TEM images show that the $LiYbF_4$:30%Tb core-only UCNPs are roughly spherical with a mean size of 12.2 ± 0.6 nm (Fig. 1c and S3†), while the $LiYbF_4$:2%Er UCNPs synthesized under identical conditions are rhombohedral with a mean size of (16.9 ± 0.8) × (21.7 ± 1.3) nm (Fig. 1d and S4†). This indicates that the doping concentration of Ln^{3+} has a significant impact on the size and morphology of the resulting UCNPs. Meanwhile, it was found that the size and morphology of the UCNPs can be tuned through the control of reaction time and/or temperature. For example, the mean size of the resulting $LiYbF_4$:2%Er UCNPs can be tuned from (12.5 ± 1.1) × (15.5 ± 0.9) nm to (16.9 ± 0.8) × (21.7 ± 1.3) nm by elevating the reaction temperature from 300 °C to 320 °C (Fig. S5†). Similarly, by lengthening the reaction time from 20 min to 2 h at 320 °C, the mean size of the UCNPs can be tuned from 7.5 ± 0.8 nm to (17.5 ± 1.4) × (22.4 ± 1.6) nm, with their morphology evolving from spherical to rhombohedral (Fig. S6†). Such a morphology evolution of $LiYbF_4$:Ln^{3+} UCNPs is ascribed to the anisotropic growth of the tetragonal NPs, which agrees well with our previous observations in $LiLuF_4$:Ln^{3+} and $LiYF_4$:Ln^{3+}.[40,41]

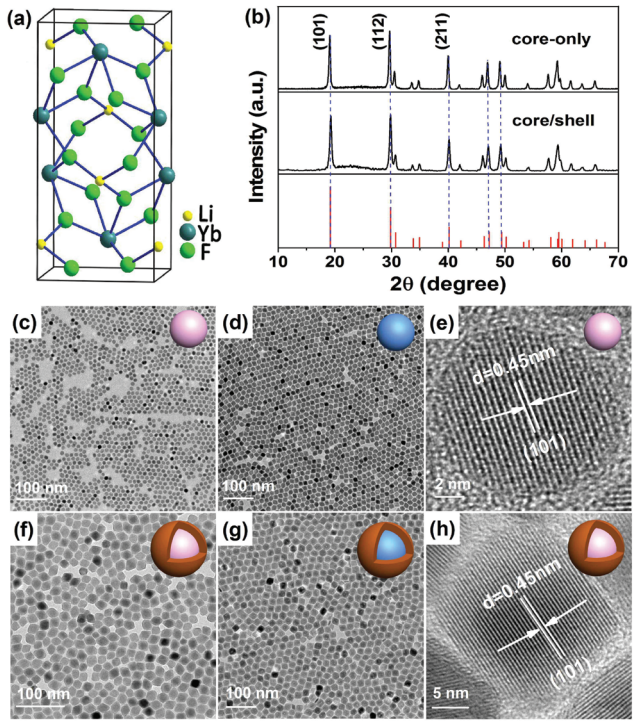

Fig. 1 (a) Crystal structure of tetragonal $LiYbF_4$. (b) XRD patterns of $LiYbF_4$:30%Tb core-only and $LiYbF_4$:30%Tb@$LiYF_4$ core/shell UCNPs. The bottom lines show the standard XRD pattern of tetragonal $LiYbF_4$ (JCPDS No. 71-1211). TEM images of (c) $LiYbF_4$:30%Tb and (d) $LiYbF_4$:2% Er core-only UCNPs synthesized at 320 °C for 1 h, and (f) $LiYbF_4$:30% Tb@$LiYF_4$ and (g) $LiYbF_4$:2%Er@$LiYF_4$ core/shell UCNPs synthesized in a core/shell precursor ratio of 1 : 1. (e, h) The corresponding HRTEM images for (c) and (f).

In addition to core-only UCNPs, core/shell UCNPs with a tunable shell thickness from ~2 nm to ~7 nm were also synthesized by controlling the ratio of the core/shell precursors through epitaxial growth of an inert $LiYF_4$ shell around the core (Fig. S7†). The TEM images (Fig. 1f and g) show that both $LiYbF_4$:30%Tb@$LiYF_4$ and $LiYbF_4$:2%Er@$LiYF_4$ core/shell UCNPs synthesized in a core/shell precursor ratio of 1 : 1 are rhombohedral with their mean sizes of (20.0 ± 0.9) × (26.2 ± 1.2) nm and (25.3 ± 1.6) × (30.2 ± 1.7) nm (Fig. S3 and S4†), respectively. The core/shell structure can be verified by the discernible contrasted TEM image and high-angle annular dark-field scanning TEM (HAADF-STEM) analysis of the core/shell UCNPs (Fig. S3 and S4†). The high crystallinity of both core-only and core/shell UCNPs was further confirmed by the intense selected area electron diffraction (SAED) ring patterns (Fig. S3†) and the high-resolution TEM (HRTEM) images (Fig. 1e and h) which exhibit clear lattice fringes with an observed d spacing of 0.45 nm for the (101) plane of tetragonal $LiYbF_4$. Compositional analysis by EDS revealed the Yb, Y and F elements of the matrix and the Tb and Er elements of the dopant (Fig. S3 and S4†). The absence of Li is because of its small atomic number (M = 3) that cannot be detected by EDS. More importantly, the modified high-temperature co-precipitation method can be extended to the synthesis of other Ln^{3+}-doped UCNPs, especially those heterovalently doping with Ln^{3+} that were difficult to synthesize before, such as cubic $KMgF_3$:Ln^{3+} and orthorhombic $BaMgF_4$:Ln^{3+} (Fig. S8†).

3.2 Non-cooperative sensitization upconversion from Er^{3+}, Ho^{3+}, and Tm^{3+}

Under 980 nm NIR laser irradiation, intense yellow, green and blue UCL can be observed in colloidal cyclohexane solution of the UCNPs doped with Er^{3+}, Ho^{3+} and Tm^{3+}, respectively, which became much brighter after coating by an inert $LiYF_4$ shell (Fig. 2). The corresponding UCL spectra show that all the UCNPs exhibit sharp and characteristic emission peaks, which can be exclusively attributed to the intra-$4f^N$ electronic transitions of Er^{3+}, Ho^{3+} and Tm^{3+}, respectively (Fig. 2b–d). With increasing the particle size, the UCL intensity of the UCNPs was gradually enhanced due to the reduced surface quenching effect, as a result of the decreased surface-to-volume ratio of the UCNPs.[42] For example, the integrated UCL intensity of $LiYbF_4$:2%Er core-only UCNPs was remarkably enhanced by a factor of 14 upon increasing their particle size from ~7.5 nm to ~(17.5 × 22.4) nm (Fig. S9†). However, the corresponding UCL lifetimes of $^4S_{3/2}$ (0.17 ms) and $^4F_{9/2}$ (0.19 ms) of Er^{3+} were observed nearly unchanged (Fig. S10†), which contradicts with the common viewpoint that the UCL lifetime of Ln^{3+} generally decreases with the decrease in particle size.[43,44] Such a size-independent UCL decay behavior in stoichiometric Yb-containing systems may originate from very fast energy migration among Yb^{3+} sub-lattices, as also evidenced by the observation of a nearly unchanged DSL lifetime (0.18 ms) of $^2F_{5/2}$ of Yb^{3+} (Fig. S10†).[23]

To further improve the UCL, we passivated the surface of the UCNPs by growing an inert $LiYF_4$ shell around the core (Fig. 2a). It was found that the integrated UCL intensity of $LiYbF_4$:2%Er@$LiYF_4$ core/shell UCNPs underwent an initial increase and then decreased with the increase in the shell thickness (Fig. S11†). This can be attributed to a synergic effect of the increased isolation of the core from its environment and the decreased Yb^{3+} absorption arising from the increased shell thickness.[41,45] The integrated UCL intensity of the core/shell UCNPs with optimal shell thicknesses was enhanced by a factor of approximately 970, 7 and 6 for Er^{3+}, Ho^{3+} and Tm^{3+}, respectively, in comparison with their core-only counterparts (Fig. 2b–d). Accordingly, the UCL lifetimes of $^4F_{9/2}$ of Er^{3+}, $^5F_5$ of Ho^{3+} and $^1D_2$ of Tm^{3+} and the DSL lifetime of $^2F_{5/2}$ of Yb^{3+} were found to increase from 0.19, 0.21, 0.19 and 0.18 ms to 0.35, 1.00, 0.43 and 1.20 ms, respectively (Fig. S12–S15†). Besides, it was observed that all the UCL decays displayed a rising edge in the initial stage, as a result of the slow population process of the emitting energy levels through ET from Yb^{3+}, thus revealing the ETU mechanism for the non-cooperative sensitization UCL of Er^{3+}, Ho^{3+} and Tm^{3+} in $LiYbF_4$ (Fig. S16†).[28,46] Both the enhanced UCL intensity and lengthened lifetime in core/shell UCNPs unequivocally confirm the effective surface passivation that alleviates the deleterious surface quenching effect. The absolute UCQY, defined as the ratio of the number of emitted photons to the number of absorbed photons, was determined to be 3.36 ± 0.06%, 0.69 ± 0.01% and 0.81 ± 0.06% for Er^{3+}, Ho^{3+} and Tm^{3+}, respectively, in core/shell UCNPs upon 980 nm NIR laser excitation at a power density of 70 W cm^{-2} (Table S2†).

More importantly, we observed that, under 980 nm excitation at a low power density of 5 W cm^{-2}, the ratio of the UCL intensity of the UV emission at ~362 nm to the NIR emission at ~800 nm ($R_{UV/NIR}$) in $LiYbF_4$:1%Tm was unusually larger (*e.g.*, 0.14 *vs.* 0.02 in $NaYbF_4$:Tm) than that in other Tm^{3+}-activated UCNPs, such as $NaYF_4$:Yb,Tm, $NaYbF_4$:Tm, and $LiYF_4$:Yb,Tm (Fig. S17†).[40,47,48] This can be attributed to the unique crystal structure of $LiYbF_4$ and the energy migration process through Yb^{3+} sub-lattices to nearby Tm^{3+} ions that promotes the high-order multiphoton UCL of Tm^{3+}.[36,49] The intense UCL in the UV region is highly desired for triggering the photochemical reactions in several promising biomedical applications, such as the remote control of drug delivery and cell adhesion,[50–52] thus offering the great potential of $LiYbF_4$:Ln^{3+} UCNPs as effective UCL nano-bioprobes in the field of biomedicine.

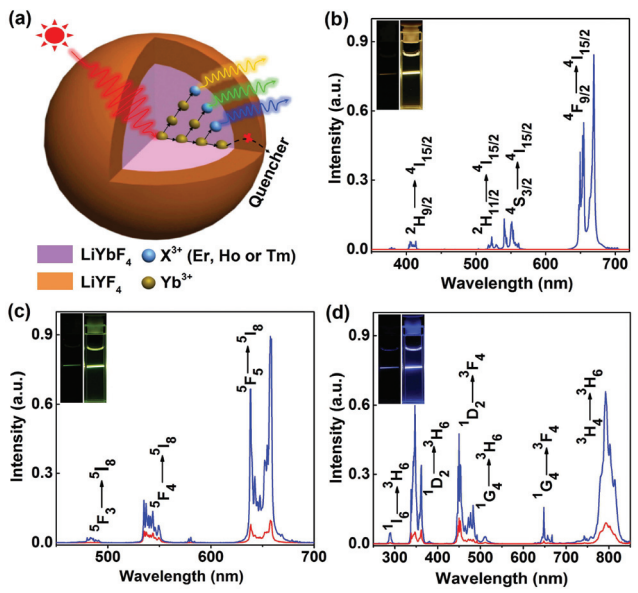

Fig. 2 (a) Schematic illustration of the ET process in $LiYbF_4$:Ln^{3+}@$LiYF_4$ core/shell UCNPs. RT UCL spectra of (b) $LiYbF_4$:2%Er^{3+}, (c) $LiYbF_4$:2% Ho^{3+} and (d) $LiYbF_4$:1%Tm^{3+} core-only (red) and core/shell (blue) UCNPs with an optimal shell thickness of $LiYF_4$ upon NIR excitation at 980 nm. The insets show the corresponding UCL photographs for the colloidal cyclohexane solution of the UCNPs (~5 mg mL^{-1}) under 980 nm NIR laser irradiation at a power density of 10 W cm^{-2}.

3.3 Cooperative sensitization upconversion from Tb^{3+}

Apart from ETU from Er^{3+}, Ho^{3+} and Tm^{3+}, we also investigated the CSU process in $LiYbF_4$:Tb^{3+} UCNPs. To realize effective CSU in $LiYbF_4$, the doping concentration of Tb^{3+} was first optimized to be 30 mol%, by considering the concentration quenching of Tb^{3+} and the doping-induced particle size variation (Fig. S18†). Under 980 nm NIR irradiation, green UCL can be explicitly observed in colloidal cyclohexane solution of both $LiYbF_4$:30%Tb core-only and $LiYbF_4$:30%Tb@$LiYF_4$ core/shell UCNPs (Fig. 3b). The UCL spectra show that all the emission peaks can be exclusively assigned to the $^5D_4$ (or $^5D_3$) → ^7F_J

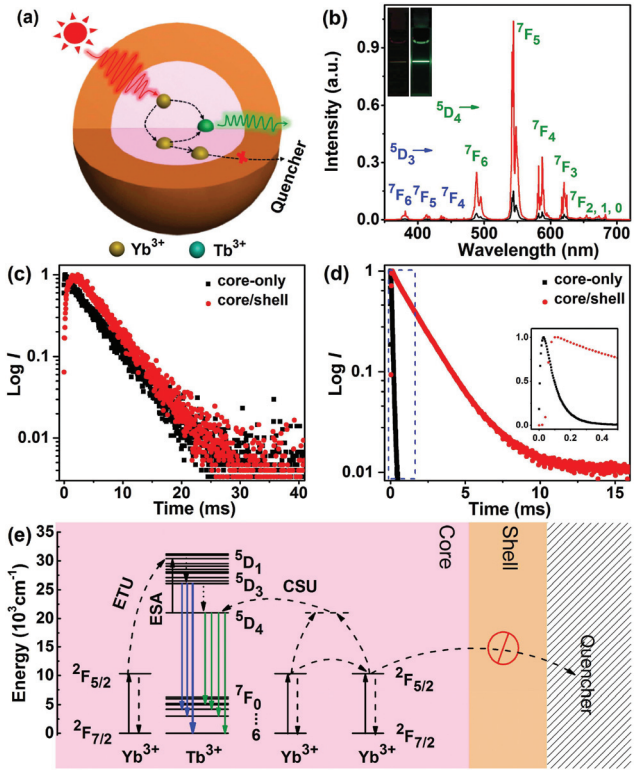

Fig. 3 (a) Schematic illustration of the ET process in $LiYbF_4$:Tb^{3+}@$LiYF_4$ core/shell UCNPs. (b) RT UCL spectra of $LiYbF_4$:30%Tb^{3+} core-only and core/shell UCNPs upon NIR excitation at 980 nm. The insets show the corresponding UCL photographs for the colloidal cyclohexane solution of the UCNPs (~5 mg mL^{-1}) under 980 nm NIR laser irradiation at a power density of 20 W cm^{-2}. (c) UCL decays from $^5D_4$ of Tb^{3+} by monitoring the Tb^{3+} emission at 544 nm under 980 nm excitation, and (d) DSL decays from $^2F_{5/2}$ of Yb^{3+} by monitoring the Yb^{3+} emission at 980 nm under 940 nm excitation in $LiYbF_4$:30%Tb^{3+} core-only and $LiYbF_4$:Tb^{3+}@$LiYF_4$ core/shell UCNPs. (e) Schematic energy level diagrams showing the CSU processes for Tb^{3+} *via* the cooperative sensitization of Yb^{3+}. The dashed, dotted and full arrows represent the ET, non-radiative relaxation and radiative transition processes, respectively.

(J = 6, 5, 4 and 3) transitions of Tb^{3+}, and the integrated UCL intensity of Tb^{3+} is ~7 times enhanced for core/shell UCNPs relative to their core-only counterparts (Fig. 3b), as a result of the reduced surface quenching effect.[42] The UCL decays from $^5D_4$ of Tb^{3+} display a rising edge in the initial stage followed by a single-exponential decay with a fitted lifetime of 6.17 ± 0.01 ms for both core-only and core/shell UCNPs (Fig. 3c). The rising edge in the decay curve reflects the slow population process of $^5D_4$ of Tb^{3+} through ET from Yb^{3+}, which is dictated by the PL decay from $^2F_{5/2}$ of Yb^{3+}.[28,46] The lengthening in the rising edge of the decay curve for core/shell UCNPs is consistent with the PL lifetime lengthening of Yb^{3+} (from 0.12 ms to 1.87 ms, Fig. 3d), thus confirming the ET process from Yb^{3+} to Tb^{3+}. The exactly same decay time of $^5D_4$ of Tb^{3+} for core-only and core/shell UCNPs is ascribed to the large energy gap (14 714 cm^{-1}) between $^5D_4$ and its next low-lying level $^7F_0$ of Tb^{3+}, which requires more than 30 lattice phonons to bridge and thus prevents Tb^{3+} from surface quenching.[53] The unchanged decay time of Tb^{3+} and the significantly lengthened decay time of Yb^{3+} confirm that the surface quenching effect in $LiYbF_4$:Ln^{3+} core-only UCNPs originates mainly from energy migration through the Yb^{3+} sub-lattice to surface defects or high-energy vibrational groups surrounding the UCNPs (Fig. 3a).

Because the energy difference between $^5D_4$ of Tb^{3+} and $^2F_{5/2}$ of Yb^{3+} is too large (~10 304 cm^{-1}) to be compensated by lattice phonons of the matrix (*e.g.*, 460 cm^{-1} in $LiYbF_4$),[54] resonant or phonon-assisted ET from Yb^{3+} to Tb^{3+} hardly occurs. Therefore, it is generally assumed that the ET from Yb^{3+} to Tb^{3+} is a second-order cooperative sensitization process, where the energy of a pair of excited Yb^{3+} is transferred simultaneously to an adjacent Tb^{3+}.[19] Once Tb^{3+} is excited to $^5D_4$, it can be further excited to $^5D_1$ through absorption of a pump photon (excited-state absorption, ESA) or through ET from a third Yb^{3+} (ETU), thus enabling the population of $^5D_3$ and thereby its emission through non-radiative relaxation from $^5D_1$ (Fig. 3e). The two-photon UCL from $^5D_4$ and three-photon UCL from $^5D_3$ of Tb^{3+} were further corroborated by the number of pump photons (n) responsible for the corresponding UC emissions, namely, 1.75 ± 0.05 and 2.28 ± 0.05 for $^5D_4 \rightarrow {}^7F_J$ (J = 6, 5, 4 and 3) and $^5D_3 \rightarrow {}^7F_J$ (J = 6, 5 and 4) transitions, respectively (Fig. S19†). The deviation from the theoretically predicted photon number for the population of $^5D_4$ (n = 2) and $^5D_3$ (n = 3) of Tb^{3+} is most probably due to the UC saturation caused by the middle-to-high pump power density regime we employed.[55,56] The absolute UCQY for CSU, which had never been reported before, was determined to be 0.0085 ± 0.0035% in $LiYbF_4$:Tb^{3+}@$LiYF_4$ core/shell UCNPs upon 980 nm NIR laser excitation at a power density of 70 W cm^{-2}. This QY value for CSU is around 2–3 orders of magnitude lower than that for non-cooperative sensitization ETU in $LiYbF_4$:Ln^{3+} UCNPs (Table S2†), which is in agreement with the theoretical prediction that CSU is 2–3 orders of magnitude less efficient than ETU.[11]

3.4 Excited-state dynamics involved in the CSU process

To gain more insights into the CSU process in $LiYbF_4$:Tb^{3+} UCNPs, we recorded the temperature-dependent steady-state and transient UCL spectra of Tb^{3+}. It was found that the integrated UCL intensity of Tb^{3+} increased significantly with temperature rise (Fig. 4a and b). Typically, the integrated UCL intensity of Tb^{3+} at RT is approximately one order of magnitude stronger than that at 10 K. This is in marked contrast with the observation that the integrated DSL intensities of Tb^{3+} and Yb^{3+} showed a decrease with temperature rise (Fig. 4b, S20 and S21†). The decrease in the DSL intensity is due mainly to the larger non-radiative transition probability at higher temperatures, as well documented in most Ln^{3+}-doped phosphors.[57] Because the only difference between the UCL and DSL from $^5D_4$ of Tb^{3+} lies in their excitation channels, namely, cooperative ET (CET) from Yb^{3+} in UCL and non-radiative relaxation from $^5D_1$ of Tb^{3+} in DSL, the anomalous increase in the integrated UCL intensity with temperature rise can be ascribed to the temperature-dependent CET process from Yb^{3+}.[29–31] By means of high-resolution optical spectroscopy at 10 K, the

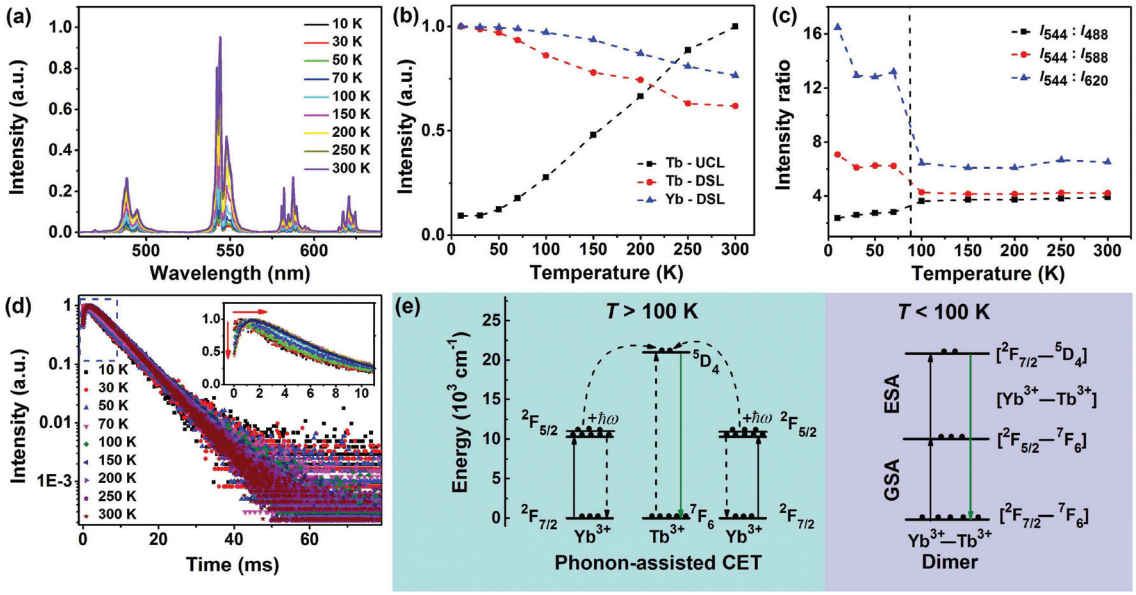

Fig. 4 (a) Temperature-dependent UCL spectra of $LiYbF_4$:30%Tb^{3+}@$LiYF_4$ core/shell UCNPs upon NIR excitation at 980 nm. (b) Normalized integrated UCL intensity of Tb^{3+} and DSL intensities of Tb^{3+} and Yb^{3+} as a function of temperature. (c) Ratio of the integrated UCL intensities of $^5D_4 \rightarrow {}^7F_5$ (544 nm) to $^5D_4 \rightarrow {}^7F_6$ (488 nm), $^7F_4$ (588 nm), and $^7F_3$ (620 nm) transitions of Tb^{3+} as a function of temperature. (d) Temperature-dependent UCL decays from $^5D_4$ of Tb^{3+} by monitoring the Tb^{3+} emission at 544 nm under 980 nm excitation. The inset shows the rising edges of the decay curves. (e) Schematic illustration showing the simplified energy levels of Yb^{3+} and Tb^{3+}, and the proposed ET processes for the population of $^5D_4$ of Tb^{3+} involved in the CSU process in $LiYbF_4$:Tb^{3+} UCNPs.

lowest Stark sub-levels of $^5D_4$ of Tb^{3+} and $^2F_{5/2}$ of Yb^{3+} were determined to be 20 597 cm^{-1} and 10 277 cm^{-1}, respectively, by assuming that all Ln^{3+} ions occupy a single site with a symmetry of S_4 in $LiYbF_4$ (Fig. S21 and S22†). In fact, we have identified a single occupant site symmetry of S_4 for Ln^{3+} ions in similar $LiLuF_4$ nanocrystals by using Eu^{3+} as the structural probes (unpublished data). As a consequence, there exists an energy mismatch of 43 cm^{-1} between the lowest Tb^{3+} $^5D_4$ level and twice the lowest Yb^{3+} $^2F_{5/2}$ level, which indicates that the CET from Yb^{3+} to Tb^{3+} requires the assistance of lattice phonons. This value of energy mismatch is close to the UCL activation energy (~128 cm^{-1}) determined from the Arrhenius plot of the natural logarithm of the normalized integrated UCL intensity of Tb^{3+} *versus* the inverse of temperature (Fig. S23†), thus verifying that the abnormal temperature-dependent UCL of Tb^{3+} is caused by the phonon-assisted CET process.[30] At higher temperatures, higher Stark sub-levels of $^2F_{5/2}$ of Yb^{3+} ions are thermally populated (Fig. S21†), from which CET occurs (Fig. 4e).[29–31]

Meanwhile, it is worth emphasizing that the UCL branching ratios of $^5D_4 \rightarrow {}^7F_J$ (J = 6, 5, 4 and 3) transitions of Tb^{3+} exhibited also a dependence on temperature with a typical transition point at ~100 K (Fig. 4c). For instance, the ratio of the integrated intensity of $^5D_4 \rightarrow {}^7F_5/{}^5D_4 \rightarrow {}^7F_3$ transitions is nearly a constant with a value of ~6.4 for T > 100 K, whereas it turns out to be ~13.2 at 30–100 K and ~16.5 at 10 K. This is very different from the DSL of Tb^{3+} where the PL branching ratios of $^5D_4 \rightarrow {}^7F_J$ (J = 6, 5, 4 and 3) transitions show only slight changes with temperature rise (Fig. S20†). The change in the UCL branching ratios for T < 100 K indicates that the electronic configuration of Yb^{3+} could be mixed into the $^5D_4$ multiplet of Tb^{3+} that modifies its transition probability to lower ^7F_J levels.[30,31,58] This can be further corroborated from the temperature-dependent UCL transients. It was observed that all the UCL decays from $^5D_4$ of Tb^{3+} exhibited a single exponential decay with fitted decay times ranging from 6.39 ms to 6.97 ms at 10–300 K (Fig. 4d and Table S3†). The nearly identical decay time at different temperatures is ascribed to the large energy gap (14 714 cm^{-1}) between $^5D_4$ and $^7F_0$ of Tb^{3+}, which makes Tb^{3+} less influenced by non-radiative relaxation. Furthermore, it was observed that the rising edge in the initial stage of the decay curve gradually shortened with the decrease of temperature, and disappeared when the temperature fell below 30 K (inset of Fig. 4d and Table S3†). The increase of rise time at higher temperatures is due to the increased population on $^5D_4$ of Tb^{3+} from Yb^{3+},[59] which agrees well with the improved UCL intensity of Tb^{3+}, thus confirming the phonon-assisted CET process. The absence of the rising edge in the decay curves at temperatures below 30 K suggests that a direct ESA process is involved in the population of $^5D_4$ of Tb^{3+}.[60] Since Tb^{3+} has no intermediate level matching that of Yb^{3+}, a reasonable ESA channel within the pair levels of weakly coupled Yb^{3+}–Tb^{3+} dimers is proposed: [Yb^{3+}:$^2F_{7/2}$–Tb^{3+}:$^7F_6$] → [Yb^{3+}:$^2F_{5/2}$–Tb^{3+}:$^7F_6$] → [Yb^{3+}:$^2F_{7/2}$–Tb^{3+}:$^5D_4$] (Fig. 4e), as established by Güdel *et al.* in $Cs_3Tb_2Br_9$:Yb^{3+} single crystals.[59,60] This well interprets the significant change in the UCL branching ratios of Tb^{3+} for T < 100 K, and also substantiates our assumption that the electronic configuration of Yb^{3+} could be mixed into the $^5D_4$ multiplet of Tb^{3+}. Based on the above analysis, we can now unambiguously unravel the underlying excited-state dynamics involved in the CSU process in $LiYbF_4$:Tb^{3+} UCNPs:

for $T > 100$ K, phonon-assisted CET is dominant; for $T < 100$ K, a sequence of two cooperative absorption steps, namely, ground-state absorption (GSA)/ESA within a weakly coupled Yb^{3+}–Tb^{3+} dimer dominates (Fig. 4e). Typically, for $T = 10$ K, the role of phonon-assisted CET is negligible due to the very small occupation number of the phonon states in the host, as verified by the negligibly weak emission at 960 nm from the second higher Stark sub-level of $^2F_{5/2}$ of Yb^{3+} (Fig. S21†).

4. Conclusions

In summary, we have systematically investigated the cooperative and non-cooperative sensitization UC in $LiYbF_4$:Ln^{3+} core-only and core/shell UCNPs. Energy migration among Yb^{3+} sublattices has been demonstrated to play a key role in the UC processes of Ln^{3+} in $LiYbF_4$, which not only resulted in the unusually strong ETU in the UV region from Tm^{3+}, but also promoted the CSU from Tb^{3+}. Particularly, we have quantified the first CSU efficiency with an absolute UCQY of 0.0085 ± 0.0035% and revealed the dominant mechanisms of phonon-assisted CET ($T > 100$ K) and sequential dimer GSA/ESA ($T < 100$ K) for the CSU process in $LiYbF_4$:Tb^{3+} UCNPs. The NIR-triggered CSU luminescence from Tb^{3+} that is free of surface quenching might exhibit great potential for applications in a variety of UCL biosensing such as homogeneous UC-FRET bioassays, despite its current limitation with extremely low efficiency. We believe that such a limitation can be circumvented by screening host materials with suitable lattice constants and phonon energies, or by confining the energy migration in a Tb^{3+}-doped shell based on smart core/shell nanostructured design, in an effort to markedly promote the three-body CSU process. The modified high-temperature co-precipitation method can be extended to the synthesis of other Ln^{3+}-doped UCNPs that were difficult in the synthesis before, which may offer a new avenue for the exploration of Ln^{3+}-doped UCNPs towards versatile biomedical applications.

Acknowledgements

This study is supported by the 973 program of MOST (no. 2014CB845605), the NSFC (No. U1305244, 21325104, and 21501180), the CAS/SAFEA International Partnership Program for Creative Research Teams, the Strategic Priority Research Program of the CAS (No. XDB20000000), the Youth Innovation Promotion Association (No. 2016277), the Chunmiao Project of Haixi Institutes of the CAS (No. CMZX-2016-002), and Natural Science Foundation of Fujian Province (No. 2015J05116, 2017J05095, and 2017I0018).

References

1 G. F. Wang, Q. Peng and Y. D. Li, *Acc. Chem. Res.*, 2011, **44**, 322–332.
2 J. C. G. Bünzli and S. V. Eliseeva, *Chem. Sci.*, 2013, **4**, 1939–1949.
3 G. Y. Chen, H. L. Qiu, P. N. Prasad and X. Y. Chen, *Chem. Rev.*, 2014, **114**, 5161–5214.
4 W. Zheng, P. Huang, D. T. Tu, E. Ma, H. M. Zhu and X. Y. Chen, *Chem. Soc. Rev.*, 2015, **44**, 1379–1415.
5 B. Zhou, B. Y. Shi, D. Y. Jin and X. G. Liu, *Nat. Nanotechnol.*, 2015, **10**, 924–936.
6 D. M. Yang, P. A. Ma, Z. Y. Hou, Z. Y. Cheng, C. X. Li and J. Lin, *Chem. Soc. Rev.*, 2015, **44**, 1416–1448.
7 X. J. Zhu, W. Feng, J. Chang, Y. W. Tan, J. C. Li, M. Chen, Y. Sun and F. Y. Li, *Nat. Commun.*, 2016, **7**, 10437.
8 M. K. Tsang, W. W. Ye, G. J. Wang, J. M. Li, M. Yang and J. H. Hao, *ACS Nano*, 2016, **10**, 598–605.
9 Y. Li, J. L. Tang, D. X. Pan, L. D. Sun, C. Y. Chen, Y. Liu, Y. F. Wang, S. Shi and C. H. Yan, *ACS Nano*, 2016, **10**, 2766–2773.
10 Y. Mita, *J. Appl. Phys.*, 1972, **43**, 1772–1778.
11 F. Auzel, *Chem. Rev.*, 2004, **104**, 139–173.
12 M. Haase and H. Schafer, *Angew. Chem., Int. Ed.*, 2011, **50**, 5808–5829.
13 G. K. Liu, *Chem. Soc. Rev.*, 2015, **44**, 1635–1652.
14 J. F. Suyver, J. Grimm, M. K. van Veen, D. Biner, K. W. Krämer and H. U. Güdel, *J. Lumin.*, 2006, **117**, 1–12.
15 F. Wang, R. R. Deng, J. Wang, Q. X. Wang, Y. Han, H. M. Zhu, X. Y. Chen and X. G. Liu, *Nat. Mater.*, 2011, **10**, 968–973.
16 H. Dong, L.-D. Sun and C.-H. Yan, *Chem. Soc. Rev.*, 2015, **44**, 1608–1634.
17 L. Tu, X. Liu, F. Wu and H. Zhang, *Chem. Soc. Rev.*, 2015, **44**, 1331–1345.
18 F. W. Ostermayer and L. G. Van Uitert, *Phys. Rev. B: Solid State*, 1970, **1**, 4208–4212.
19 F. Auzel, *J. Lumin.*, 1990, **45**, 341–345.
20 G. S. Maciel, A. Biswas and P. N. Prasad, *Opt. Commun.*, 2000, **178**, 65–69.
21 H. S. Wang, C. K. Duan and P. A. Tanner, *J. Phys. Chem. C*, 2008, **112**, 16651–16654.
22 W.-P. Qin, Z.-Y. Liu, C.-N. Sin, C.-F. Wu, G.-S. Qin, Z. Chen and K.-Z. Zheng, *Light: Sci. Appl.*, 2014, **3**, e193.
23 Q. Q. Su, S. Y. Han, X. J. Xie, H. M. Zhu, H. Y. Chen, C.-K. Chen, R.-S. Liu, X. Y. Chen, F. Wang and X. G. Liu, *J. Am. Chem. Soc.*, 2012, **134**, 20849–20857.
24 R. R. Deng, J. Wang, R. F. Chen, W. Huang and X. G. Liu, *J. Am. Chem. Soc.*, 2016, **138**, 15972–15979.
25 M. Xue, X. J. Zhu, X. C. Qiu, Y. Y. Gu, W. Feng and F. Y. Li, *ACS Appl. Mater. Interfaces*, 2016, **8**, 17894–17901.
26 H. Dong, L. D. Sun, Y. F. Wang, J. W. Xiao, D. T. Tu, X. Y. Chen and C. H. Yan, *J. Mater. Chem. C*, 2016, **4**, 4186–4192.
27 K. Prorok, M. Pawlyta, W. Stręk and A. Bednarkiewicz, *Chem. Mater.*, 2016, **28**, 2295–2300.
28 D. R. Gamelin and H. U. Güdel, *Top. Curr. Chem.*, 2001, **214**, 1–56.
29 M. V. D. Vermelho, P. V. dos Santos, M. T. D. Araújo, A. S. Gouveia-Neto, F. C. Cassanjes, S. J. L. Ribeiro and Y. Messaddeq, *J. Lumin.*, 2003, **102–103**, 762–767.

30 G. M. Salley, R. Valiente and H. U. Güdel, *J. Phys.: Condens. Matter*, 2002, **14**, 5461–5475.
31 L. D. Menezes, G. S. Maciel, C. B. de Araujo and Y. Messaddeq, *J. Appl. Phys.*, 2003, **94**, 863–866.
32 X. Y. Zhang, M. Q. Wang, J. J. Ding, D. L. Gao, Y. H. Shi and X. H. Song, *CrystEngComm*, 2012, **14**, 8357–8360.
33 S. Sarkar, V. Adusumalli, V. Mahalingam and J. A. Capobianco, *Phys. Chem. Chem. Phys.*, 2015, **17**, 17577–17583.
34 J. Wang, R. R. Deng, M. A. Macdonald, B. L. Chen, J. K. Yuan, F. Wang, D. Z. Chi, T. S. Hor, P. Zhang, G. K. Liu, Y. Han and X. G. Liu, *Nat. Mater.*, 2014, **13**, 157–162.
35 W. Wei, Y. Zhang, R. Chen, J. L. Goggi, N. Ren, L. Huang, K. K. Bhakoo, H. D. Sun and T. T. Y. Tan, *Chem. Mater.*, 2014, **26**, 5183–5186.
36 X. Chen, L. M. Jin, W. Kong, T. Y. Sun, W. F. Zhang, X. H. Liu, J. Fan, S. F. Yu and F. Wang, *Nat. Commun.*, 2016, **7**, 10304.
37 X. Wang, J. Zhuang, Q. Peng and Y. D. Li, *Nature*, 2005, **437**, 121–124.
38 D. M. Liu, X. X. Xu, Y. Du, X. Qin, Y. H. Zhang, C. S. Ma, S. H. Wen, W. Ren, E. M. Goldys, J. A. Piper, S. X. Dou, X. G. Liu and D. Y. Jin, *Nat. Commun.*, 2016, **7**, 10254.
39 S. Salaün, M. T. Fornoni, A. Bulou, M. Rousseau, P. Simon and J. Y. Gesland, *J. Phys.: Condens. Matter*, 1997, **9**, 6941–6956.
40 M. Wang, Z. Chen, W. Zheng, H. M. Zhu, S. Lu, E. Ma, D. T. Tu, S. Y. Zhou, M. D. Huang and X. Y. Chen, *Nanoscale*, 2014, **6**, 8274–8282.
41 P. Huang, W. Zheng, S. Y. Zhou, D. T. Tu, Z. Chen, H. M. Zhu, R. F. Li, E. Ma, M. D. Huang and X. Y. Chen, *Angew. Chem., Int. Ed.*, 2014, **53**, 1252–1257.
42 F. Wang, J. Wang and X. G. Liu, *Angew. Chem., Int. Ed.*, 2010, **49**, 7456–7460.
43 J. B. Zhao, Z. D. Lu, Y. D. Yin, C. Mcrae, J. A. Piper, J. M. Dawes, D. Y. Jin and E. M. Goldys, *Nanoscale*, 2013, **5**, 944–952.
44 W. Zheng, S. Y. Zhou, Z. Chen, P. Hu, Y. S. Liu, D. T. Tu, H. M. Zhu, R. F. Li, M. D. Huang and X. Y. Chen, *Angew. Chem., Int. Ed.*, 2013, **52**, 6671–6676.
45 X. M. Li, Z. Z. Guo, T. C. Zhao, Y. Lu, L. Zhou, D. Y. Zhao and F. Zhang, *Angew. Chem., Int. Ed.*, 2016, **55**, 2464–2469.
46 W. Q. Luo, C. Y. Fu, R. F. Li, Y. S. Liu, H. M. Zhu and X. Y. Chen, *Small*, 2011, **7**, 3046–3056.
47 G. Y. Chen, T. Y. Ohulchanskyy, R. Kumar, H. Ågren and P. N. Prasad, *ACS Nano*, 2010, **4**, 3163–3168.
48 H. Y. Xing, W. B. Bu, Q. G. Ren, X. P. Zheng, M. Li, S. J. Zhang, H. Y. Qu, Z. Wang, Y. Q. Hua, K. L. Zhao, L. P. Zhou, W. J. Peng and J. L. Shi, *Biomaterials*, 2012, **33**, 5384–5393.
49 H. L. Qiu, C. H. Yang, W. Shao, J. Damasco, X. L. Wang, H. Ågren, P. Prasad and G. Y. Chen, *Nanomaterials*, 2014, **4**, 55–68.
50 W. Li, J. S. Wang, J. S. Ren and X. G. Qu, *J. Am. Chem. Soc.*, 2014, **136**, 2248–2251.
51 Z. Y. Hou, Y. X. Zhang, K. R. Deng, Y. Y. Chen, X. J. Li, X. R. Deng, Z. Y. Cheng, H. Z. Lian, C. X. Li and J. Lin, *ACS Nano*, 2015, **9**, 2584–2599.
52 W. P. Fan, B. Shen, W. B. Bu, X. P. Zheng, Q. J. He, Z. W. Cui, K. L. Zhao, S. J. Zhang and J. L. Shi, *Chem. Sci.*, 2015, **6**, 1747–1753.
53 T. Miyakawa and D. L. Dexter, *Phys. Rev. B: Solid State*, 1970, **1**, 2961.
54 S. A. Miller, H. E. Rast and H. H. Caspers, *J. Chem. Phys.*, 1970, **52**, 4172–4175.
55 M. Pollnau, D. R. Gamelin, S. R. Luthi, H. U. Güdel and M. P. Hehlen, *Phys. Rev. B: Condens. Matter*, 2000, **61**, 3337–3346.
56 J. F. Suyver, A. Aebischer, S. Garcia-Revilla, P. Gerner and H. U. Güdel, *Phys. Rev. B: Condens. Matter*, 2005, **71**, 125123.
57 G. Blasse and B. C. Grabmaier, *Luminescent Materials*, Springer-Verlag, Berlin, 1994.
58 G. Amaranath, S. Buddhudu and F. J. Bryant, *J. Non-Cryst. Solids*, 1990, **122**, 66–73.
59 G. M. Salley, R. Valiente and H. U. Güdel, *J. Lumin.*, 2001, **94–95**, 305–309.
60 G. M. Salley, R. Valiente and H. U. Güdel, *Phys. Rev. B: Condens. Matter*, 2003, **67**, 134111.